

## Vortex-loop crinkling in the three-dimensional $XY$ model: Numerical evidence in support of an ansatz

Biplab Chattopadhyay, Mangal C. Mahato, and Subodh R. Shenoy

*School of Physics, University of Hyderabad, Hyderabad 500134, Andhra Pradesh, India*

(Received 16 July 1992; revised manuscript received 13 January 1993)

A scaling theory for the three-dimensional (3D)  $XY$  ferromagnet was previously proposed, in terms of directed vortex loops of average diameter  $a = e^l$ , and core size  $a_c(l)$ . An ansatz was made for the loop self-energy from a  $1/R$  potential,  $E \sim a \ln[a/a_c(l)] \rightarrow a \ln K_l^{-x}$ , where  $K_l$  is the screened coupling and  $x \approx 0.6$  the self-avoiding random-walk exponent. Here, the central role of the core-size ansatz in producing known 3D  $XY$  exponents is brought out in numerical solutions of the scaling equations. We then relate the cutoff  $a_c(l)$  to radial fluctuations around the mean radius  $a/2$ , and provide partial numerical support for the ansatz by computer-generated vortex-loop configurations. A Flory-type polymer argument for the core size  $a_c(l)$  is given.

### I. INTRODUCTION

The general notion of a phase transition driven by topological excitations was proposed by Berezinskii<sup>1</sup> and Kosterlitz and Thouless,<sup>2</sup> in the context of the 2D  $XY$  ferromagnet. The topological excitations are vortex points, of topological "charge"  $\pm 1$ , interacting via a  $\log(R)$  potential. The charges are bound in dipoles in the low-temperature phase and form a screened, unbound plasma of charges, in the high-temperature phase. The vortex-point unbinding picture was applied to 2D helium films,<sup>3</sup> 2D superconductors,<sup>4</sup> 2D Josephson arrays,<sup>5</sup> and 2D melting.<sup>6</sup> The 2D systems do not have long-range order, or conventional exponents, at transition.

The idea that vortex loops may drive the 3D superfluid-helium transition was suggested by Onsager and Feynman.<sup>7</sup> Shockley proposed a picture of 3D melting involving the proliferation of dislocation loops.<sup>7</sup> The extension of topological scaling ideas to a 3D transition with conventional long-range order, was carried out by Williams<sup>8</sup> and Shenoy,<sup>9</sup> who adapted 2D nested-scaling procedures<sup>10</sup> of Kosterlitz, and of Young, to 3D directed loops with  $1/R$  segment-segment interaction. An application of the ideas to hydrodynamic vortices in turbulent flows has been made recently.<sup>11</sup>

Numerical simulation<sup>12</sup> of the 3D  $XY$  model showed that vortex loops do exist, and proliferate at transition. This was extended to the layered 3D  $XY$  model,<sup>13</sup> of interest<sup>14</sup> in the context of high- $T_c$  superconductors. Simulations of the isotropic  $XY$  model were made by Kohring, Shrock, and Wills.<sup>15</sup> They showed that an external chemical potential that suppressed the vorticity in each lattice square, also suppressed the transition out of the ordered state, i.e., raised the transition temperature. This is of obvious current relevance.<sup>9(b),14</sup>

Thus, 3D  $XY$  vortex loops are present,<sup>12,13</sup> are involved in the transition,<sup>15</sup> and a real-space scaling approach exists.<sup>8,9</sup> An important part of the argument<sup>9</sup> is incomplete, however.

The scaling treatment focuses on quasicircular directed loops characterized by some average "diameter"  $a \equiv e^l$  with a short-distance, scale-dependent cut-off  $a_c(l)$  associated with the "crinkling" or fluctuation around "a." Due to vector cancellation between segments, the effective perimeter " $\pi a$ " is less than or equal to the actual perimeter  $P$  along the segments. The picture is that of a toroidal region with a circular loop axis, containing the radial fluctuations<sup>11</sup> roughly inside this "core" size  $a_c$ . The self-energy of the loop is taken to be<sup>9</sup>

$$\beta E_l = \pi^2 K_l a \ln[a/a_c(l)]. \quad (1.1)$$

Here  $K_l$  is the dressed coupling constant at scale "a."

The scale-dependent core size  $a_c(l)$  is modeled as follows. The ratio of the core size to the effective diameter is taken to be a function of the dressed coupling  $K_l$ , that influences the folding and crinkling. The dependence on  $K_l$ , close to the critical point,  $l \approx l_- = \ln(T - T_c)^{-\nu} \gg 1$ , is taken to be a power  $\sim K_l^x$ . (Here  $\nu$  is the exponent of the loop size blowout, that is also the spin-spin correlation length exponent.) Due to approximate vector cancellation of the potential between nearly antiparallel segments, the loop wandering in the core region is like a self-avoiding random walk (SAW). Since  $K_l$  scales as a length, it is natural to take  $x = 0.6$ , the SAW exponent<sup>16</sup> in 3D. Thus this core-size model or ansatz assumed valid for  $l \approx l_-$  yields the self-energy as

$$\beta E_l = \pi^2 K_l a \ln(K_l^{-x}). \quad (1.2)$$

For  $K_l \rightarrow K^* = 0.3875$ , the fixed-point value, reached for  $l = l_- \rightarrow \infty$ , one has,  $\beta E_l \equiv \pi K^* E$ , with

$$E/a \approx 1.78. \quad (1.3)$$

A purely finite core model, with a circular loop, yields a transition, but with  $\nu = 0.5$ , as the mean-field exponent. The model for the expanding core  $a_c(l) \sim a$ , also yields the transition, but now with critical exponents and coupling close to accepted values;<sup>17</sup>  $\nu = 0.6717$ ,  $\alpha = -0.015$ .

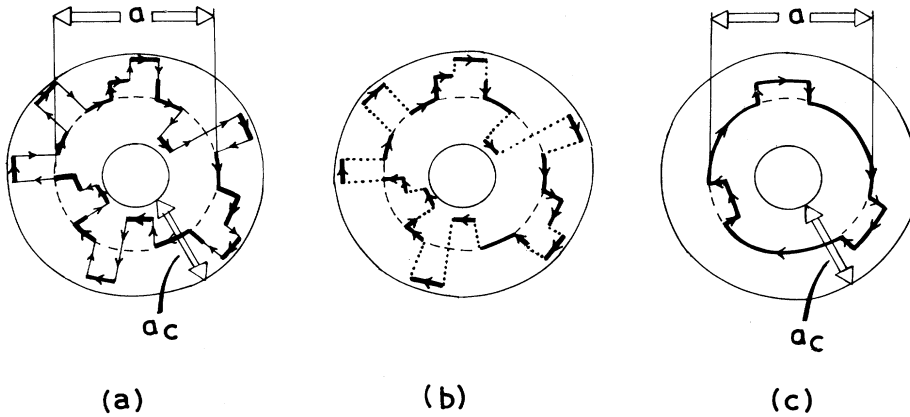


FIG. 1. Schematic picture of equivalent topological current distributions, as seen at large distances (a). Full loop with mean diameter “ $a$ ,” transverse fluctuations “ $a_c$ ,” and uncanceled azimuthal segments of narrow radial fluctuations (bold-face). (b) Uncanceled segments. (c) Effective loop, of mean diameter “ $a$ ” and arc cutoff “ $a_c$ .”

In this paper we carry out numerical simulations clarifying the meaning of the scaling procedure and of the effective diameter  $a$ , providing partial support for the core-size ansatz. More precisely we do the following. (a) We solve the scaling equations numerically with and without the ansatz, showing its central role in producing the correct exponents. (b) From the theoretical self-energy expression, the core size  $a_c(l)$  is related to the transverse root-mean-square (rms) radial fluctuation ( $\sigma$ ), with  $\sigma \propto a$ , the mean-loop diameter. (c) We numerically generate vortex-loop configurations, by randomly replacing bonds by elementary radial fluctuations<sup>11</sup> to generate crinkled loops, starting from a regular square loop as a seed. We find that the random configurations have an associated “best-fit” circle with a mean diameter  $a \sim P^\delta$ ,  $\delta \simeq 0.4$ , where  $P$  is the loop perimeter. The scaled self-energy  $E$ , both from the full energy expression and the approximated form, is proportional to the diameter,

$$E \simeq (0.40 \pm 0.25)a . \quad (1.4)$$

Thus the overall loop-scaling approach is made more plausible. (d) A handwaving Flory-type polymer argument for  $a_c$  is made

The paper is organized as follows. In Sec. II we reformulate and restate the scaling argument for general configuration loops. In Sec. III we show that the cutoff  $a_c(l)$  can be related to transverse segment fluctuations, and present the Flory argument. Section IV summarizes the results and discusses possible future work.

## II. THE VORTEX-LOOP SCALING ARGUMENT AND ROLE OF THE ANSATZ

The  $\pm$  vortex unbinding transition in 2D is pictured as follows. There are a few tightly-bound dipoles (of positive creation energy) at very low temperatures. As the temperature is raised, the dipoles, interacting via a  $\log(R)$  potential, expand, and more and more screening dipoles can fit in between them. This weakens the binding still further, and the dipoles can further expand, until a blowout, or dipole unbinding occurs at  $T = T_{\text{BKT}}$ . Screening of the  $\log(R)$  potential sets in at  $T_{\text{BKT}}$ , from the  $\pm 1$  two-component plasma formed by unbinding of the most weakly bound pairs of the largest size and ener-

gy. Thus the transition is led, not by the most probable small-dipole configurations of lowest energy, but by the less probable, most unstable, large-dipole configurations.<sup>2</sup>

The extension of this 2D picture to the topological excitations of the 3D  $XY$  model is pictured as follows. There are a few tightly-bound vortex loops (with those of interest having positive creation energy), at very low temperatures. As the temperature is raised, the loops, with a  $1/R$  segment-segment interaction, expand, and more and more nested loops can fit in between. This weakens the binding still further, and the loops can further expand, until a blowout, or loop unbinding occurs at  $T = T_c$ . Screening of the  $1/R$  potential sets in at  $T = T_c$ , from the random wandering of the infinite-sized loops. The transition is dominated by the expansion and unfolding of the most weakly-bound loops of the largest size  $\sim \xi_- \sim (T_c - T)^{-\nu}$ , and energy. Thus the transition is led, not by the most probable, lowest energy, tightly folded or smallest loops, but by the less probable, most unstable, more extended or quasicircular loops.<sup>8,9</sup>

A vortex loop of perimeter  $P$  on the 3D lattice may be thought of as a closed chain with hinged segments. The segments have arrows  $\mathbf{J}$  on them, all the way round the chain, with the energy depending on the cosine,  $\mathbf{J}_r \cdot \mathbf{J}_{r'}$ , of the angle between segments, favoring backward folding or antiparallel sections. The highest energy state is clearly a fully pulled-out chain, forming a circle, and the lowest, a tightly folded ball with lots of antiparallel segments giving negative contributions to the energy. For adjacent segments pointing in the same direction, the  $\mathbf{J} \cdot \mathbf{J}$  interaction will favor the segments to swing perpendicular to each other making the interaction energy zero, rather than positive. Four successive  $90^\circ$  bonds of unit segments form an elementary radial fluctuation. By “radial fluctuation,” we mean in general a “transverse fluctuation” with radial and azimuthal components. Such fluctuations can merge, and extend into a larger structure. Thus the relatively high-energy family of loops that lead the unbinding will retain a quasicircular character, in the sense that they can be characterized by, a mean effective diameter “ $a$ ”. However, there will be a spread of loop foldings or radial fluctuations over a core region of size  $\sim a_c$  around this constant- $a$  circle. (Note that by “core” we do not mean to imply<sup>13(a)</sup> any new repulsive short-range interaction.) The loop configurations would thus be in a toroidal region with a small hole [Fig. 1(a)].

Such configurations would have nonzero dipole moments, just as a planar “current” loop would. A family of decreasing-diameter loops could be nested, with consequent screening of the larger loops driving the transition.

The maximum such loop size is  $a \sim \xi_- \sim |\epsilon|^{-\nu}$  where  $|\epsilon| = |T - T_c|/T_c$ , and  $\nu = \frac{1}{2}$  for circular loops alone.<sup>9</sup> If  $a_c/a \rightarrow 0$  for  $l = l_- \equiv \ln(\xi_-) \rightarrow \infty$ , then the loop crinkling would be irrelevant, and would not change the critical exponents. We have made a critical-behavior ansatz for  $l \leq l_-$ , the largest dressed loop,  $a_c(l)/a \simeq K_l^x$ , where  $K_l$  is the dressed coupling and  $x = 0.6$  is the Flory self-avoiding walk exponent in 3D. Then for  $l = l_- \rightarrow \infty$ ,  $a_c/a = a_c(l_-)/\xi_- = (K^*)^x = \text{const}$ , and  $a_c$  is relevant, yielding an exponent  $\nu = 0.672$ . The investigation of this ansatz or model for the core size and of the effective diameter is the subject of this paper.

In what sense can a complex, current loop distribution be characterized by a single length  $a$ ? We consider non-crossing and SAW loop configurations, for reasons given later. The potential at a point  $r$  from the topological current distribution  $\{\mathbf{J}(r')\}$  depicted in Fig. 1(a) is  $\sim \mathbf{J}(r) \cdot \sum_r \mathbf{J}(r')/|\mathbf{r} - \mathbf{r}'|$ , with origin at the center of mass, say. Not all the segments comprising the perimeter  $P$  will contribute appreciably to the potential at large  $r \gg r'$ . Consider contributions from segments which are on the adjacent sides of long narrow radial fluctuations of width  $W_h$ , that start and end at the mean circle of diameter “ $a$ .” For  $r \gg a \gg W_h$ , the contribution will tend to cancel, falling off rapidly with distance. The potential will be approximately from uncanceled segments that do not have canceling partners in the (total) vector sum of  $\mathbf{J}(r')$  in the fluctuation. Those uncanceled segments precisely span a total distance equal to the separation of the open ends of the fluctuation. If a best-fit sphere is drawn of a diameter “ $a$ ” chosen to minimize the deviation of the squared radial distance  $(\sigma/2) = \sum_{r=1}^P (r - a/2)^2/P$  of all the segments, then the uncanceled azimuthal contributions from each radial fluctuation will be scattered on or around this surface [Fig. 1(b)]. If these directed segments are moved radially to the sphere surface and added vectorially, they will form a closed curve  $\sim a \ll P$  [Fig. 1(c)]. For points far away from the current distribution,  $a/r \ll 1$ , the potential from the complex current pattern will be approximately that from this quasicircular loop

$$Z = \sum_{\{\mathbf{J}\}} \prod_L y_0^{(L)} \exp \left[ -(\pi K_0/2) \sum_{L \neq L'} \sum_{r, r'} \mathbf{J}^{(L)}(r) \cdot \mathbf{J}^{(L')}(r') U(\mathbf{r} - \mathbf{r}') \right], \quad (2.3)$$

config

where closure,  $\sum_r \mathbf{J}_\mu^{(L)}(r) = 0$  has been used. The fugacity  $y_0^{(L)}$  of loop  $L$  is determined by the loop self-energy segment-segment interaction on the same loop ( $L = L'$ )

$$y_0^{(L)} = \exp \left[ -(\pi K_0/2) \sum_{r \neq r'} \mathbf{J}^{(L)}(r) \cdot \mathbf{J}^{(L)}(r') \tilde{U}(\mathbf{r} - \mathbf{r}') \right]. \quad (2.4)$$

For circles of perimeter  $P$ , the self-energy  $\sim P \ln P/P_c$ , with the  $\sim \sum [\mathbf{J}^{(L)}(r)]^2 U(0) \sim U(0)P$  contribution absorbed in the cutoff  $P_c$ . We consider similar, relatively

from which long narrow radial fluctuations have been eliminated. As far as the outside world is concerned, the complex vortex-loop configuration could be represented only by a loop of effective diameter  $a$ .

The diameter “ $a$ ” will increase with the total perimeter  $P$ , but only as  $P \sim a^\delta$ ,  $\delta < 1$ , with the remaining length in the perimeter going into radial fluctuations that do not affect other or far-away loops. The value of  $\delta$  is not important for the loop-scaling argument above, that deals with loops  $L$  of various effective diameter  $\{a_L\}$  and not actual perimeters  $\{P_L\}$ . However, we find  $\delta \sim 0.4$ .

For calculations of the self-energy of large loops, the dominant contribution will also be from these uncanceled segments, that mimic a circular loop, of scaled self-energy  $E \sim a \ln[a/a_c(l)]$ . The cut-off  $a_c(l)$  is a length outside of which one may ignore the detailed radial fluctuation structure and represent the configuration only by its effective circular loop. The paired segments of long, narrow radial fluctuations have only a short-range interaction with other parts of the same, or other, radial fluctuations. It is thus not unreasonable that this region  $\sim a_c$  might be related to the random-walk exponent of a short-range repulsive polymer.

We now briefly review the renormalization procedure that leads to the scaling equations, presented in detail elsewhere,<sup>9</sup> and clarify the meaning of the effective scale  $a$ .

The 3D XY model on a cubic lattice (of lattice constant  $a_0 = 1$ ) is

$$\beta H = -K_0 \sum_{\langle ij \rangle} \cos(\theta_i - \theta_j), \quad -\pi < \theta_i < \pi. \quad (2.1)$$

It can be mapped<sup>18</sup> via a dual transformation onto directed vortex loops, with topological current  $J_\mu(r) = 0, \pm 1, \dots$ , and directions  $\mu = 1, 2, 3$ . The loops interact via a Biot-Savart law with flipped sign:

$$\beta H = (\pi K_0/2) \sum_{r \neq r'} \mathbf{J}(r) \cdot \mathbf{J}(r') \tilde{U}(\mathbf{r} - \mathbf{r}'), \quad (2.2)$$

where  $\tilde{U}(R) \equiv U(R) - U(0)$ , and  $\nabla^2 U(R) = -4\pi\delta(\mathbf{R})$  with  $U(R) \sim R^{-1}$ . The topological current is locally conserved,  $\Delta \cdot \mathbf{J}(r) = 0$ ,  $\forall r$ , i.e., the loops are closed.

The loops can be labeled by  $L$ , with interacting segments on different loops  $L \neq L'$  entering the loop-loop interaction:

opened-out (but crinkled) quasicircular configurations, of positive total interaction energy. The nonbacktracking loop configurations are characterized by a length  $a_L$  with  $a_L \geq a$ , the minimum-size loop diameter, defining the scale  $a \equiv e^l$ . As discussed above and in the next section, for  $L = 1$  (smallest loop size,  $a_1 = a$ ) the fugacity can be written as

$$y^{(L=1)} \equiv y_l \simeq \exp[-\pi^2 K_l a \ln(a/a_c(l))]. \quad (2.5)$$

This is the small-expansion parameter in the problem,  $y_l \ll 1$ . For the bare original scale, the smallest circle is

chosen<sup>9</sup> to fit into the smallest square plaquette of side  $a_0=1$ , so that the minimum separation of circular vortex loops is the lattice constant. The bare cut-off is chosen to be  $a_c(0)=0.5652$ , based on the calculation of helium vortex-core energies, and this lattice match.

The partition function is evaluated<sup>9</sup> in the Kosterlitz-Thouless low-density approximation, by successively integrating out nested configurations in the scale range  $a, a+da$ , starting from  $a_0$ . This is schematically depicted in Fig. 2(a). Note that we integrate out the smaller loops at all distances from larger segments, including zero separation. Loop crossing can occur, with locally perpendicular segments.<sup>19</sup> However, for consistency in the successive integration of scales, a large loop that involves a self-crossing forming a small bubble must be classified as two simple noncrossing loops, one large, one small, that happen to touch. We can thus, without loss of generality and to avoid double counting consider only noncrossing simple loops as the basic units in the scaling. The configurations considered in the self-energies are, thus closed, nonbacktracking, vectorically labeled and self-avoiding (SAW) random walks. The  $XY$  model is mapped onto a polymer-type problem.

We formally separate the partition function  $Z$  contributions into those ( $Z|_>$ ) only of minimum loop separation  $>a$ , and contributions ( $\delta Z$ ) from interactions of the smallest  $a, a+da$  loops with these:

$$Z = Z|_> + \delta Z. \quad (2.6)$$

The incremental partition function contributions, expanding the Boltzmann factor, and with  $\mathbf{r}_{1,2}$  locating segments in a shell,  $a, a+da$ , are given by

$$\delta Z = \sum_{J=\pm 1} y_l^2 \int \frac{d^3 r_1}{a^3} \int \frac{d^3 r_2}{a^3} \prod_{L \neq L'} \prod_{r, r' (\neq r_1, r_2)} [1 - (\pi/2) K_l \mathbf{J}^{(L)}(r) \cdot \mathbf{J}^{(1)}(r_1) \times \{U(\mathbf{r}-\mathbf{r}_1) - U(\mathbf{r}-\mathbf{r}_1^*)\}] \times [1 - (\pi/2) K_l \mathbf{J}^{(L')}(r') \cdot \mathbf{J}^{(1)}(r_2) \times \{U(\mathbf{r}'-\mathbf{r}_2) - U(\mathbf{r}'-\mathbf{r}_2^*)\}], \quad (2.7)$$

where in (2.7)  $y_l$  is the smallest loop fugacity at a general scale, starting from  $y_{l=0}=y_0$  and we have suppressed writing weight factors of direct  $\mathbf{J}(r) \cdot \mathbf{J}(r')$  interactions of loops larger than  $a+da$ .

The screening configurations are as shown in Fig. 2(b). In (2.7) we have used the fact that for a closed loop, for every directed segment  $\mathbf{J}_\mu(r_1)$ , there is somewhere an oppositely directed segment at  $\mathbf{r}_1^*$ , of maximal separation  $|\mathbf{r}_1 - \mathbf{r}_1^*|$ , such that  $\mathbf{J}_\mu(r_1) = -\mathbf{J}_\mu(r_1^*)$  [see Fig. 2(b)]. For a planar circular loop, where  $\mathbf{R}_0$  locates the center of mass, and  $\mathbf{r}_1 = \mathbf{R}_0 + \boldsymbol{\rho}_1$  there is an opposite segment across the diameter, at  $\mathbf{r}_1^* = \mathbf{R}_0 + \boldsymbol{\rho}_1^* = \mathbf{R}_0 - \boldsymbol{\rho}_1$ . Thus, from the closed loop nature of screening one has a ‘‘derivative’’  $U(\mathbf{r}-\mathbf{r}_1) - U(\mathbf{r}-\mathbf{r}_1^*) \sim -(\mathbf{r}_1 - \mathbf{r}_1^*) \cdot \nabla_{\mathbf{r}_1} U(\mathbf{r}-\mathbf{r}_1)$  occurring in (2.7). Integrating out configurations in (2.7), the first-order  $\sim \nabla U$  terms vanish by symmetry, over all loop orientations, and only  $\sim \nabla U \cdot \nabla U$  terms survive, with the average  $\langle (\mathbf{r}_1 - \mathbf{r}_1^*) \cdot (\mathbf{r}_2 - \mathbf{r}_2^*) \rangle \sim \langle (\mathbf{r}_1 - \mathbf{r}_1^*)^2 \rangle \sim a^2$ , defining a mean-equivalent ‘‘diameter’’ even for crinkled, wandering loops. The ‘‘diameter’’ or loop scale is thus a ‘‘best-fit’’ to the actual loop configuration, as discussed, and found in computer-generated loops later.

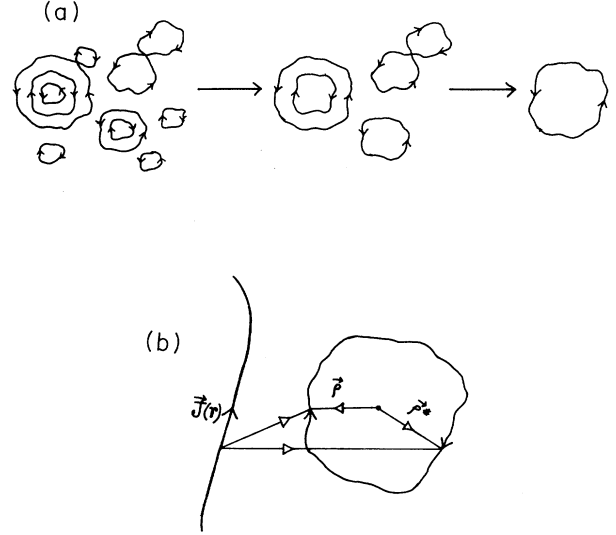


FIG. 2. (a) Schematic diagram to show the loop scaling at each interaction. Loops are incrementally integrated out, starting from the smallest loop size. Note that complex loops formed from crossing are regarded as simple loops that are touching. (b) Diagrammatic representation of screening of far-off segments through loops of smaller size. Note that for every  $\mathbf{J}$  at  $\boldsymbol{\rho}$  measured from the center of mass, there is a  $-\mathbf{J}$  in the small loop at position  $\boldsymbol{\rho}^*$ . There is a similar interaction with another segment  $\mathbf{J}(r')$ , not shown.

With a partial integration, the  $\sim \nabla U \cdot \nabla U$  terms go as  $\sim U \nabla^2 U \sim U$ , since the interaction is essentially the inverse Laplacian  $U \sim \nabla^{-2}$ . The whole procedure is a straightforward generalization of the 2D vortex-point

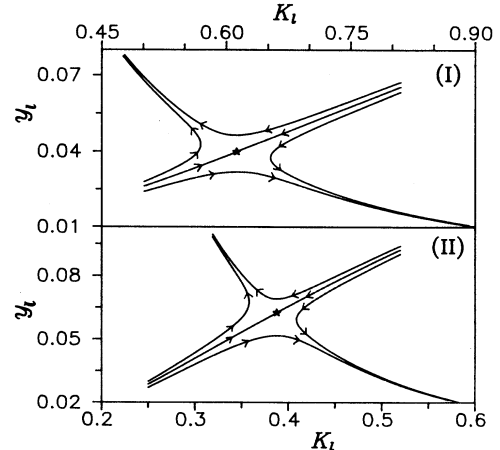


FIG. 3. Renormalization flows of  $y_l$  vs  $K_l$  for case I (without ansatz) and case II (with ansatz).

scaling of Kosterlitz,<sup>10</sup> where the  $\pm 1$  bound dipole pairs are successively integrated out, with the opposite-sign dipole charges similarly yielding the “derivatives” acting on  $U \sim \nabla^{-2} \sim \ln(R)$ .

The above procedure generates the incremental contribution to the partition function, on reexponentiating the  $O(dl)$  terms:

$$\delta Z = \sum_{\{J\}} \left\{ -\frac{\pi^3}{2} K_l^2 y_l dl \sum_{L \neq L'} \sum_{r, r'} \mathbf{J}^{(L)}(r) \cdot \mathbf{J}^{(L')}(r') U(r-r') \right\} \\ \times \exp \left[ -\frac{\pi}{2} K_l \sum_{L \neq L'} \sum_{r, r'} \mathbf{J}^{(L)}(r) \cdot \mathbf{J}^{(L')}(r') U(r-r') \right] \\ \times \prod_L y_l^{(L)} \quad (2.8)$$

where smallest-scale  $L=1$  contributions do not occur, and free-energy corrections<sup>9</sup> are dropped for simplicity. Here, we have restored writing the  $\mathbf{J}(r) \cdot \mathbf{J}(r')$  weight factors for scales  $> a+da$ . We can now recombine  $\delta Z$  with  $Z|_>$  (that is (2.8) with curly bracket set equal to unity)

and reexponentiate  $O(dl)$  terms. A rescaling of all explicit scale dependence in  $Z$  regenerates a partition function of the same form, but with corrections  $\sim dl$  absorbed in the renormalized coupling and fugacity,  $K_{l+dl}$  and  $y_{l+dl}$ , respectively. The scaling equations are<sup>8,9</sup>

$$\frac{dK_l}{dl} = K_l - A_0 y_l K_l^2, \quad (2.9a)$$

$$\frac{dy_l}{dl} = (6 - \pi^2 K_l L_l) y_l, \quad (2.9b)$$

with  $A_0 = 4\pi^3/3$  and  $L_l$ , a factor from the scale dependence of the ansatz for  $a_c(l)$  in the self-energy,  $L_l = 1 - x \ln(K_l)$ . If  $a_c/a$  is not taken to be scale dependent through  $K_l$ , then  $x=0$  and  $L_l=1$ .

The scaling equations have been solved analytically<sup>9</sup> by linearizing about the fixed point,  $K^* = 0.3875$  and  $y^* = 0.062$ . They can also be solved numerically both with [ $L_l = 1 - x \ln(K_l)$ ], and without ( $L_l = 1$ ), the ansatz. Figure 3 shows the renormalization flows with and without the ansatz. In all cases, the  $L_l = 1$  approximation

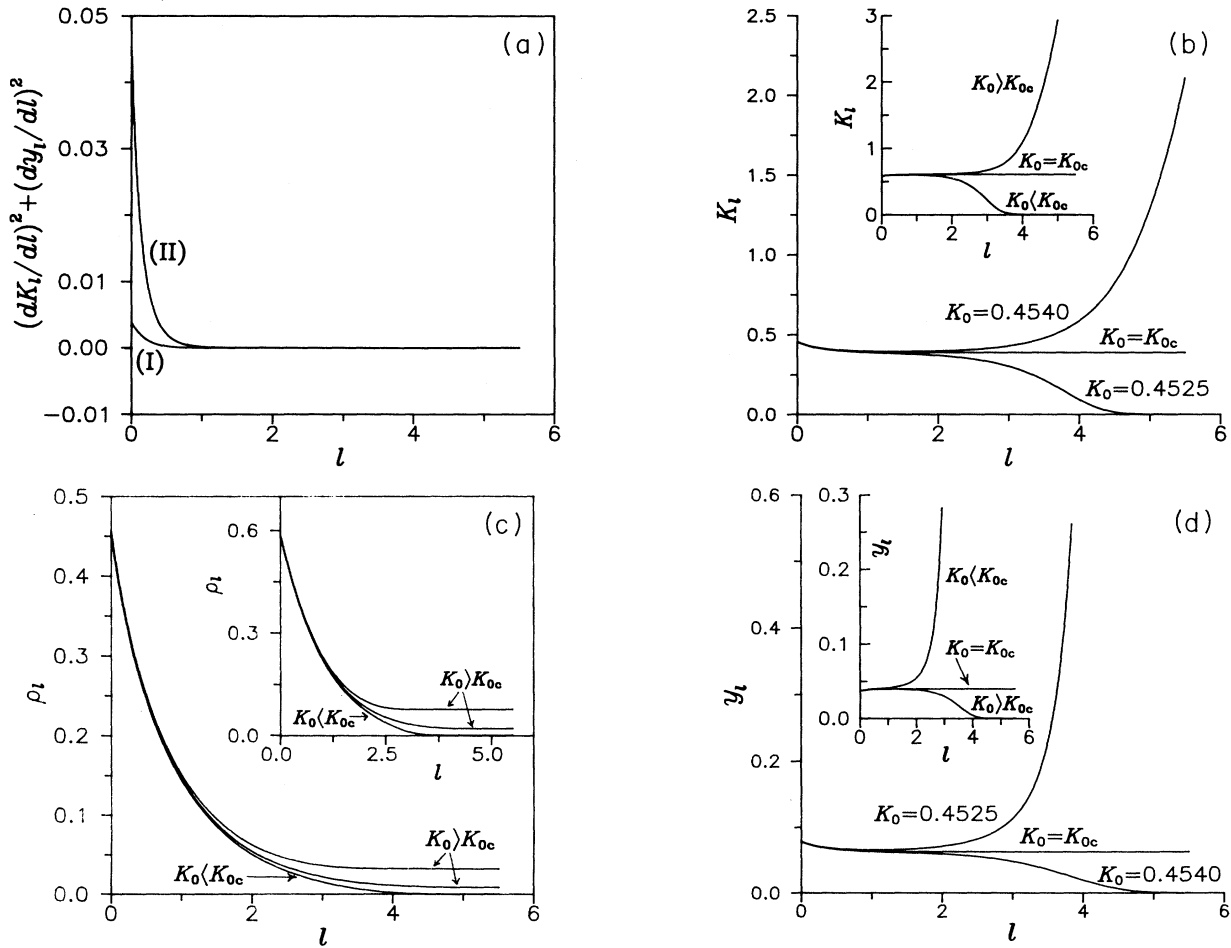


FIG. 4. (a) Plot of  $S_l = (dk_l/dl)^2 + (dy_l/dl)^2$  vs  $l$ . Curve (I) is for without ansatz ( $L_l=1$ ) and (II) is for with ansatz [ $L_l = 1 - 0.6 \ln(K_l)$ ]. In both the cases  $K_0 = K_{0c}$ , the critical value. (b) Plot of loop coupling  $K_l$  vs  $l$  around, and at, the critical point. (Inset: the same without the ansatz.) (c) Plot of superfluid density  $\rho_l \equiv K_l e^{-l}$  vs  $l$ . (Inset: without ansatz.)  $\rho_s$  is the asymptotic value. (d) Plot of loop fugacity  $y_l$  vs  $l$  around, and at, the critical point. (Inset: without ansatz.)

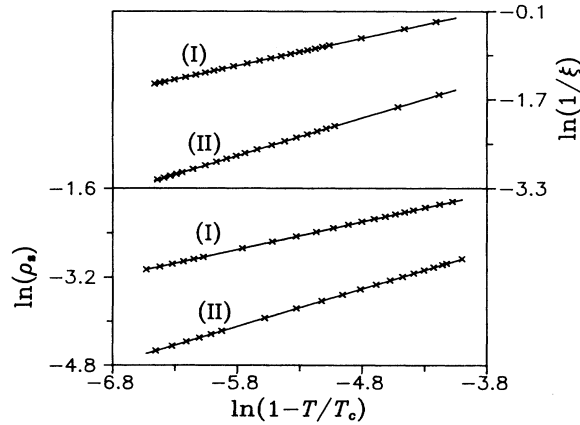


FIG. 5. Here  $\ln(\rho_s)$  [ $\rho_s$ =flattened out value of superfluid density  $\rho_l$  as  $\epsilon \ll 1$ ], and  $\ln(1/\xi_-)$  [ $\xi_-$ =correlation length  $\sim a/\ln(y_l)$  at  $l=l_- \gg 1$ ] are plotted vs  $\ln(\epsilon)$  [ $\epsilon=(T_c-T)/T_c$ ]. In both the plots curves (I) and (II) are without and with the ansatz.

gives the qualitative behavior. The scale-dependent core-size model only provides an adjustment that gives better quantitative results.

We define a quantity  $S_l=(dK_l/dl)^2+(dy_l/dl)^2$  that vanishes only when both coupled scaling equations have a fixed point,  $(dK_l/dl)=0=(dy_l/dl)$ . This occurs asymptotically, both with and without the ansatz, at critical values  $K_{0c}=0.4535$  and  $K_{0c}=0.5858$ , respectively, as shown in Fig. 4(a). The renormalized coupling  $K_l$  increases with  $l$  for  $K_0 > K_{0c}$  ( $T < T_c$ ). [From the first term in (2.9a),  $K_l \sim K_0 e^l$ .] For  $K_0 < K_{0c}$  ( $T > T_c$ ), the coupling  $K_l \rightarrow 0$  asymptotically vanishes [see Fig. 4(b)], i.e., there is screening of the  $1/R$  segment potential. The helicity modulus (that is a superfluid density in the case of He II, of the same universality class) is proportional to<sup>9</sup>  $\rho_l \equiv K_l e^{-l}$ . In Fig. 4(c) we see that  $\rho_l$  flattens out to a nonzero constant<sup>20</sup> ( $\rho_s$ ) for  $K_0 > K_{0c}$ . For  $(K_0 - K_{0c})/K_{0c} \equiv (T_c - T)/T_c = \epsilon \ll 1$ ,  $\rho_s$  decreases to zero at the transition temperature as  $\rho_s \sim \epsilon^u$  where  $u=0.67$  or  $u=0.5$ , with and without the ansatz. Figure 4(d) shows that for  $K_0 > K_{0c}$ , where the bare interaction prevails, the loop fugacity  $y_l \rightarrow 0$  and the loops are irrelevant at large separation. For  $K_0 < K_{0c}$  the fugacity increases, i.e., loops proliferate at large scale,  $y_l \rightarrow \infty$ , providing the screening of  $K_l$  as above. The fugacity falls off exponentially below transition, defining the largest loop size  $\xi_-$ ,  $y_l \sim e^{-a/\xi_-}$ . This loop size diverges,  $\xi_- \sim |\epsilon|^{-\nu}$  as  $\epsilon \rightarrow 0$ . Figure 5 shows log-log plots of  $1/\xi_- = \ln(y_l)/a$  versus  $|\epsilon|$  as well as  $\rho_s$  versus  $|\epsilon|$  yielding exponents  $u=\nu=0.679$  and  $u=\nu=0.499$ , with, and without, the ansatz. The series solution<sup>17</sup> value  $\nu=0.678 \pm 0.005$  is close to the exponent, from vortex loop scaling. The critical vortex coupling  $K_{0c}=0.4535$  is fortuitously<sup>9,21</sup> close to the series solution<sup>17</sup> ( $K_{0c}=0.454 \pm 0.001$ ) and MC<sup>13</sup> ( $K_{0c}=0.4539$ ) values.<sup>21</sup>

Thus while  $L_l=1$  gives the qualitative features of the transition as a first approximation, the scale-dependent

core ansatz  $L_l=1-x\ln(K_l)$  is of central importance in obtaining the critical values close to accepted ones.

### III. THE CORE ANSATZ IN THE SELF-ENERGY

The ansatz for the core size  $a_c$  in the self-energy may be restated, in separate steps, as follows.

(i) Basic length scale: Topological current configurations that dominate vortex-loop unbinding have a typical length scale “ $a$ ” associated with them, related to the total perimeter  $P$  by  $a \sim P^\delta$  where  $\delta < 1$ . This length scale  $a$  is associated with the net azimuthal vorticity left after cancellation between segments that double back and forth in radial fluctuations. It is the diameter of the effective directed loop, as seen by far-off segments of other loops.

(ii) Scale-dependent cut-off: The fluctuations around this mean length produces a scale-dependent cut-off  $a_c(l)$  in the self-energy

$$\beta E_l = \pi^2 K_l a \ln[a/a_c(l)] . \quad (3.1)$$

If each part of the effective length contributed a constant value, the energy would be  $\sim a$ . The logarithmic factor comes from the  $1/R$  interaction between effective (uncanceled) segments, that are swept from between a minimum “ $a_c(l)$ ” and maximum “ $a$ ” separation.

(iii) Coupling-constant dependent core ansatz: The nature of the interaction, and the crinkling of the loops, yield a core size that is dependent on the coupling at that scale, such that, for  $l$  near the critical value  $l_- \gg 1$ ,

$$\beta E_l = \pi^2 K_l a \ln(K_l^{-x}) \equiv \pi K^* E . \quad (3.2)$$

where  $x \simeq 0.6$ , the same as the SAW exponent in 3D.

(iv) Asymptotic energy-diameter proportionality: For large loop diameters,  $\alpha \sim \xi_- \rightarrow \infty$  the scaled self-energy  $E$  is proportional to the loop diameter

$$E/a \rightarrow \pi \ln(K^*)^{-x} \simeq 1.78 . \quad (3.3)$$

Computer generation of single irregular loops must necessarily ignore the nested many-loop screening that renormalizes the coupling  $K_0 \rightarrow K_l$ , and drives the transition. Thus one can test only (i) and (iv). One expects  $E/a$  to be smaller than (3.3), since more energy-lowering crinklings are accessible, in the absence of other nested loops, that would block some of these.

We start with a square loop in the  $XZ$  plane of a 3D cubic lattice. Each time, we introduce an elementary radial fluctuation to the old configuration at a randomly chosen bond, according to rules stated below. We determine the segment interaction energy  $E \simeq \frac{1}{2} \sum_{r \neq r'} \mathbf{J}(r) \cdot \mathbf{J}(r') / |r - r'|$ , the diameter of the best-fit circle “ $a$ ” and the rms deviation around it. The key idea of a random loop as a regular seed, plus randomly inserted radial fluctuations, was used by Chorin<sup>11</sup> in the context of hydrodynamic vortices and turbulence.

Figure 6(a) shows the (elementary) radial-fluctuation insertion rules. A preexisting bond is erased if it falls between the ends of an inserted fluctuation, that can approach the bond from any of three directions. If the open ends of an inserted radial fluctuation fall on an existing bond that is part of a step, then the superimposed side is

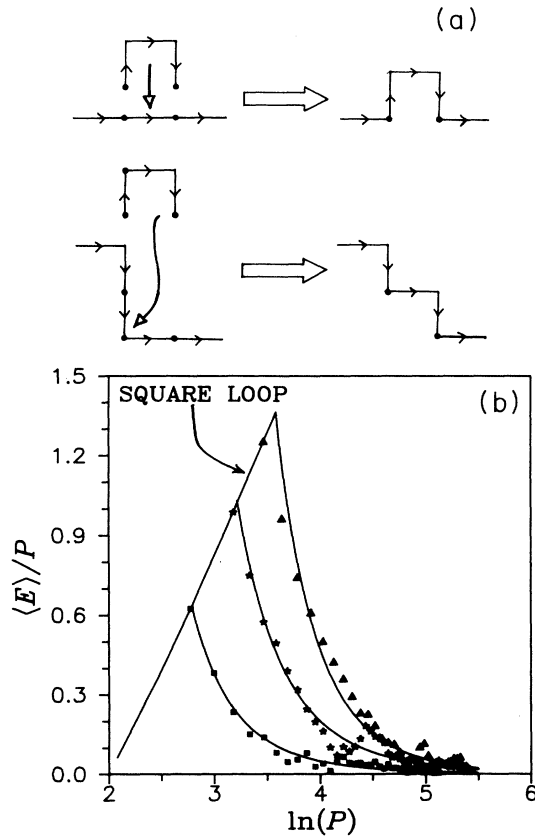


FIG. 6. (a) Diagrammatic representation of the radial fluctuation insertion rule as followed in cases of computer-generated loops. (b)  $\langle E \rangle / P$  is plotted vs  $\ln(P)$ ,  $P$ =perimeter. The straight line is for square seed configuration with increasing  $P$ .  $\langle E \rangle / P$  falls off with the insertion of radial fluctuations, for different regular starting configurations  $P=16$  (■),  $P=24$  (★),  $P=32$  (▲).

also erased. Elementary radial fluctuations can pile on top of each other, and generate long, crinkled, and winding structures, that we also call (complex) radial fluctuations. In all the transformations from the square seed, the following overall constraints are enforced: (i) bonds may not cross, so only simple, noncrossing loops are generated, as in a SAW; (ii) the direction of the original seed  $\mathbf{J}$  flow is maintained, with  $\nabla \cdot \mathbf{J} = 0$  conservation, at every site, and  $|\mathbf{J}| = 0, 1$ .

Since many trials have to be rejected, the runs have to be long. As an example, for  $E$  cut-off=0.0 we run our program with 7050 elementary radial fluctuations being inserted to a seed of perimeter 24, out of which 5400 runs are acceptable. This takes about 74 h of C.P.U. time on a Microvax II. As the run goes on, and the structure gets more involved, the probability that an insert is accepted goes down, and the diameter and core size do not change much. For example, the last 200 acceptable radial fluctuation inserts change the rms value  $\sigma$  by  $\sim 2\%$ .

Because of the  $\mathbf{J}_r \cdot \mathbf{J}_r$  factor in the interaction, an increase of total perimeter need not result in an increase of energy. In fact the radial fluctuations have antiparallel sides, and hence give a negative correction to the seed energy. The energy expression in the exponent of (2.4) gives

$E \sim P \ln(P)$ , i.e.,  $E/P \sim \ln(P)$  for regular seeds of perimeter  $P$ . The positive slope straight line of Fig. 6(b) in  $E/P$  versus  $\ln(P)$  plot confirms this. We then repeatedly insert radial fluctuations at random positions and orientations to regular seed loops of various perimeter values, and find that  $E/P$  then starts dropping. We restrict ourselves to  $E > 0$  configurations, as discussed earlier, since only the opened-out, higher energy nestable configurations will lead the transition. If by the core-size model,  $E$  actually scales as an effective diameter " $a$ " then eventually  $E/P \sim 1/P^{1-\delta}$ , accounting for the asymptotic decrease of  $E/P$  in Fig. 6(b). There is a large scatter of  $E/P$  in Fig. 6(b) for large  $P$ , indicating that the total perimeter is a poor parameter to characterize the self-energy. Very different perimeter loops can have the same energy, because of vector cancellation effects. The effective diameter  $a$  physically pictured in the previous section, is a more suitable length scale to parametrize classes of loop configurations.

We consider the various loop configurations generated on the computer. Figure 7(a) shows that the scatter of the distance  $|r|$  from the center of mass to the segments, is peaked around a mean value  $a/2$ . Defining a diameter scatter  $\sigma$  by  $\sigma^2 = \langle (2|r| - a)^2 \rangle$ , averaged uniformly over the segments of a given configuration, one finds in Fig. 7(b) that  $\sigma$  has a minimum at a "best-fit" diameter " $a$ " of that configuration. This  $a$  is found by rotating the plane of the circle on either side of the original planar seed, until a lowest minimum is reached, for that configuration. (Of course, over many configurations, this angle is as often positive as negative, since the radial-fluctuation insertions are random.) Henceforth, " $\sigma$ " and " $a$ " for a given loop, denote these optimized values. The mean diameter  $\langle a \rangle$  is found by sorting configurations into groups according to the perimeter  $P$ , and averaging over generated configurations with the same  $P$ . One finds that the mean diameter increases as a power of the perimeter  $P$

$$\langle a \rangle = P^\delta, \quad \delta = 0.4 \pm 0.003. \quad (3.4)$$

A similar result has been found by Epiney,<sup>13(a)</sup> in MC simulations. Figure 7(c) gives a plot of  $\delta = \ln(\langle a \rangle) / \ln(P)$  versus  $P$ .

We now sort configurations (of varying  $P$ ) into  $a, a + da$  bins of bin width  $da \sim 0.25$ . This defines fixed- $a$  configurations for averaging purposes. Radial fluctuations are found to be proportional to the diameter for large loops [Fig. 7(d)] with  $\langle \sigma \rangle / a = 0.49 \pm 0.01$ . The maximum fluctuation inward to the center, avoiding fluctuation from the other side, is  $\sigma \leq 0.5a$ . Thus fluctuations are close to maximal, in the absence of multiple loop nesting. Figure 7(e) shows a loop configuration, generated in 2D for illustration, with its mean diameter, and fluctuation. The actual loops are of course, generated in 3D.

As a cross-check on the role of the geometric length, we calculate the dipole moment  $|\mu| = \int d^3r \mathbf{r} \times \mathbf{J}(r)$ . For a strictly planar loop of diameter  $a$ , the moment would go as  $\mu \sim \text{diameter} \times \text{perimeter}$  for current flow, so that  $\mu \sim a^2$ . If the loop wandered totally randomly around the spherical surface, without even having the memory of a

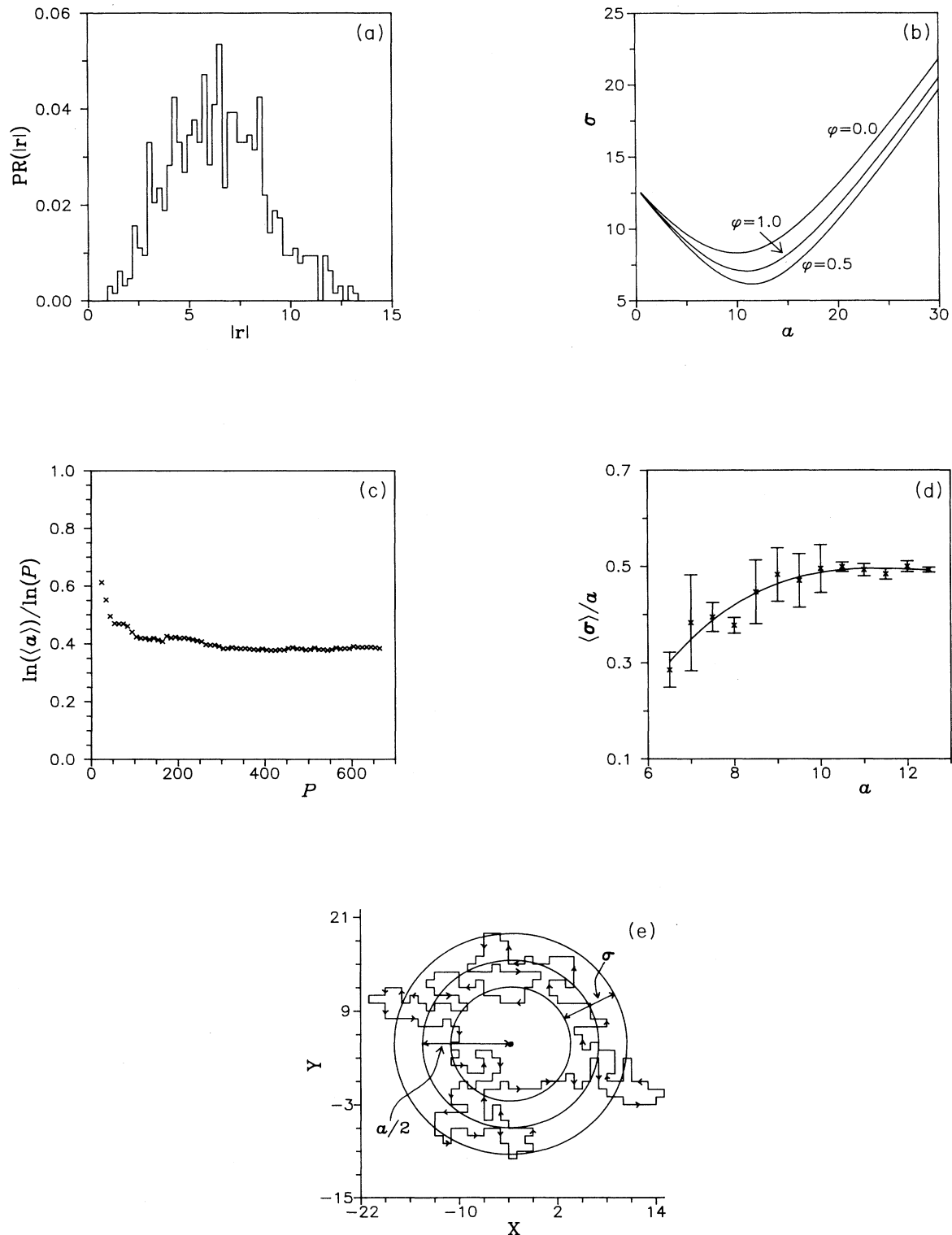


FIG. 7. (a) Histogram showing the distribution of  $|r|$  (magnitude of the distance of each segment from the center of mass) of a given computer-generated configuration. The distribution peaks around 6.0 which is consistent with the best-fit value  $a = 12.0$  for the present configuration. (b) Root-mean-square fluctuation  $\sigma$  is plotted vs chosen “ $a$ ” (diameter) values for different chosen polar angles. “ $a$ ” corresponding to minimum  $\sigma$  is taken as best-fit diameter  $a$  of the configuration. (c) Plot of  $\ln(\langle a \rangle) / \ln(P)$  vs  $P$ , showing exponent behavior. (d) Plot of  $\langle \sigma \rangle / a$  vs  $a$ , showing proportionality of diameter fluctuations and mean diameter. (e) A crinkled-loop configuration in case of 2D square lattice with best-fit circle and corresponding  $\sigma$ .

planar character, then the dipole moment  $\mu$  would be zero. For the crinkled vortex, fluctuating over a finite fraction of the spherical surface of diameter  $a$ ,  $|\mu| \sim \text{diameter} \times \text{area crisscrossed by current}$ , or  $\mu \sim a^3$ . One finds from the generated configurations that the mean moment goes as  $\mu \sim P^{1.22}$ , where the exponent is close to the expected value of  $3\delta = 1.2$ . A histogram of  $\mu/P^{1.2}$  has a dominant peak, showing that a family of excitations, scaling in the same way, does exist. In the spirit of the discussion in Sec. II this band of current region is replaced by a planar loop, for large distance potentials.

$$\langle E \rangle \simeq \pi \int \frac{d^3 r}{a^3} \int \frac{d^3 r'}{a^3} \left\langle \frac{\mathbf{J}(r) \cdot \mathbf{J}(r')}{[r^2 + r'^2 - 2rr' \cos(\theta - \theta')]^{1/2}} \right\rangle \quad (3.5)$$

where  $\mathbf{J}(r) \cdot \mathbf{J}(r') = \cos \gamma$ , and  $\gamma \equiv \theta - \theta'$ , with  $r = r' = \alpha/2$ , for a planar circle, when

$$\begin{aligned} \langle E \rangle &= \pi a \int_{\gamma_c = a_c/a}^{\pi} d\gamma \cos(\gamma) / \gamma \\ &\simeq \pi a \ln(a/a_c). \end{aligned} \quad (3.6)$$

The energy diverges, logarithmically, for segments of angular separation  $\gamma$  tending to zero requiring introduction of a cutoff  $a_c$ , i.e. a lower bound  $a_c/a$  to the angular separation. Notice from (3.5) however, that the sharp rise in  $1/R$  for neighboring segments is suppressed if the segments on the lattice are perpendicular to each other,  $\mathbf{J}(r) \cdot \mathbf{J}(r') = 0$ . Radial-fluctuation formation is thus, energetically favored. If there is a purely radial excursion  $\sim \sigma$ , linking two azimuthal direction current segments with  $\mathbf{J}(r) \cdot \mathbf{J}(r') \neq 0$ , then the divergence is again suppressed: even though  $\gamma = 0$ , the distance between the azimuthal segments is  $|r - r'| \sim \sigma$ . Thus the form of the  $\mathbf{J}(r) \cdot \mathbf{J}(r')$  interaction plays a role both in generating fluctuations, and providing a natural cut-off  $a_c$ , related to the radial fluctuation  $\sim \sigma$ .

With  $|r| \equiv r \equiv a/2 + \bar{r}$ , and performing crude truncations in (3.5),  $\bar{r}^2 \rightarrow \langle \bar{r}^2 \rangle$ ,  $\langle \bar{r}\bar{r}' \rangle = \langle \bar{r} \rangle \langle \bar{r}' \rangle = 0$ . With  $\cos \gamma \rightarrow \langle \cos(\gamma) \rangle \approx \exp(-\gamma/2K_0)$  by a Gaussian average, there is an effective upper cutoff  $\Lambda \approx 2K_0$  to the angular separation  $\gamma$ . So for a crinkled loop,

$$\begin{aligned} \langle E \rangle &\simeq \pi a \ln[(a/\langle \sigma \rangle)(\Lambda/\sqrt{2}) \\ &\quad \times \{1 + \sqrt{1/2 + 1/\Lambda^2(a/\langle \sigma \rangle)^2}\}]. \end{aligned} \quad (3.7)$$

From (3.6), one gets an expression for  $a_c(l)$  as

$$\begin{aligned} \frac{a}{a_c(l)} &\simeq [(a/\langle \sigma \rangle)(\Lambda/\sqrt{2}) \\ &\quad \times \{1 + \sqrt{1/2 + 1/\Lambda^2(a/\langle \sigma \rangle)^2}\}]. \end{aligned} \quad (3.8)$$

Since  $\langle \sigma \rangle/a$  is a constant, so is  $a/a_c(l)$ , and from (3.8), energy is proportional to the effective diameter,  $E \propto a$ , within this crude approximation.

A plot of  $\langle E \rangle/a$  versus  $a$  in Fig. 8 shows that the energy is indeed roughly proportional to the mean diameter, as in (3.3), with

$$\langle E \rangle/a \simeq 0.40 \pm 0.25 \quad (3.9)$$

The partition function, that is originally a sum over loop configurations characterized by perimeters  $\{P_L\}$ , can then be considered as a sum over configurations characterized by diameters  $\{a_L\}$ , with all possible fluctuations around them. The averages over all fluctuations around  $\{a_L\}$  are then taken as equally probable. The scaling procedure is then as given previously.

The cutoff  $a_c(l)$  is essentially the transverse loop fluctuation,  $\sigma$ , as can be seen by a rough estimate of the self-energy. The scaled self-energy, averaged uniformly over all configurations with the same mean diameter, is

with the prefactor of correct order of magnitude, and less than the nested-loop ansatz value, as expected. This means that  $\ln[a/a_c(l)]$  is indeed a constant, rather than diverging with  $\ln(a)$  as it would, if  $a \sim P$  in the regular case. The crinkling produces a scale-dependent core size  $a_c(l) \propto \alpha$ . Of course, as mentioned earlier, we cannot here simulate the full statistical mechanics to check that the detailed model  $a_c/a = (K_1)^x$ .

The importance of having closed loops was stressed in the derivation of the scaling equations. Closure is also important, in order for the self-energy to be constant for  $T < T_c$ . The potential is long range, and there is a difference between closed loops and open chains. To check the impact of closure, we have generated open-chain self-avoiding random walks using the computationally efficient pivot algorithm.<sup>22</sup> The walk will wander around isotropically about the starting point, and a purely formal "best-fit" circle to the segments around the center of mass can be defined. The geometrical  $\sigma/a$  is not changed much. But the average energy  $\langle E \rangle/a$  is drastically different: it does not level off as  $a$  increases, but keeps rising. Thus closure is important: the ansatz is for vortex loops.

Thus numerical support has been provided for the core model, clarifying the concepts involved. A simple Flory-

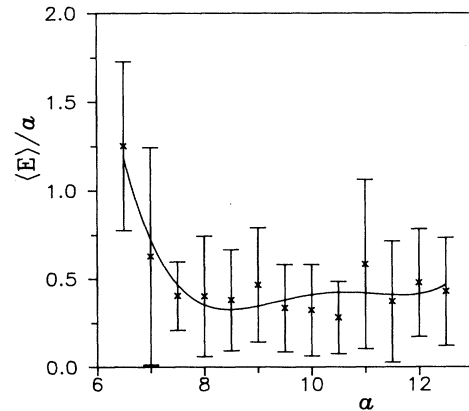


FIG. 8. Plot of  $\langle E \rangle/a$  vs  $a$  (for positive energy configurations).

type polymer argument may also be provided for  $a_c(l)$ .

In a classic argument, Flory had<sup>16(a),16(c)</sup> provided an estimate of the rms end-to-end distance  $R$  of a polymer of length  $P$ , by extremizing the free-energy contribution with respect to  $R$ . By the vector cancellation arguments of Sec. II, a radial fluctuation can be treated as a short-range interaction polymer. We follow the Flory argument closely. Consider a cylindrical region of length  $a_c$  around the best-fit circle path, passing approximately along the axis and with radius  $a_c/2$ . The volume of  $V = a_c^d$  contains randomly walking radial fluctuations of spatial extent  $\sim P_h^{1/2}$ , where  $P_h$  is the average segment length available for radial fluctuations, taken to be a finite fraction of the total perimeter,  $P_h \sim P$ . Thus the cutoff  $a_c$  is the length outside of which one can ignore fluctuation details. The radial fluctuation density is then  $\rho \sim P_h^{1/2}/a_c^d$ . The radial fluctuation interaction is then short ranged of strength<sup>16(c)</sup>  $W_0 \sim \langle \int d^d R (1 - e^{-\pi K_l J \cdot J/R}) \rangle$ , where  $\langle \rangle$  denotes an angular average. Change of variables yields  $W_0 \sim (\pi K_l)^d I$ , where  $I$  is an integral of order unity. The interaction energy for radial fluctuations is, following Flory,  $U \sim W_0 \rho^2 V$  and the entropy of the fluctuations is  $\sim -TS = a_c^2/P_h$ . The free energy is then

$$F = \frac{I(\pi K)^d P_h}{a_c^d} + \frac{a_c^2}{P_h}. \quad (3.10)$$

Extremizing, one gets, with  $P_h \sim P$ ,

$$a_c \approx K^{d/(d+2)} P^{2/(d+2)} \approx K^{0.6} P^{0.4} \quad (3.11)$$

for  $d=3$ . This is in agreement with the ansatz with an effective diameter  $a \sim P^{2/(d+2)} \sim P^{0.4}$  as in our numerical estimation.

A more rigorous argument will require a scaling out of radial fluctuations in a path integral representation<sup>16</sup> by a systematic decimation procedure. This would need a separate treatment. We have here clarified the meaning of the ansatz, and provided numerical and physical arguments to support it.

#### IV. SUMMARY AND DISCUSSION

The model for the core size  $a_c(l)$ , that enters the self-energy, and is used in the vortex-loop scaling approach

for the 3D  $XY$  model, has been given partial support, through numerical simulations and physical arguments. The importance of the ansatz in yielding quantitatively correct critical exponents is reemphasized by numerical solutions of the scaling equations. Crinkled loop configurations are generated by adding radial fluctuations randomly in 3D to regular, planar, seed configurations. Since only single loops are generated, multiloop renormalization of the coupling constant is not considered. The results are as follows. A length scale  $a \sim P^{0.4}$  can be associated with the vortex loop configurations. The self-energy scales linearly with the mean diameter. The cutoff  $a_c(l)$  can be related to fluctuations of the loop around the "best-fit" diameter "a." The constant  $\langle E \rangle/a$  for large scales is of the same order of magnitude as required by the ansatz. The ansatz  $a_c(l)/a \approx K_l^{0.6}$  can be justified by a simple Flory-type argument for the self- and mutual-avoiding radial fluctuations.

A more detailed proof would require use of polymer methods,<sup>16</sup> suitably generalized. MC simulations have been done of the angle representation of the 3D  $XY$  model,<sup>12,13,15</sup> as was done for the 2D  $XY$  model.<sup>23</sup> In the 2D case vortex points or Coulomb charges were used as the basic variables in MC simulations.<sup>24</sup> This was found to be more efficient, as each charge is a collective description of all spins. A similar MC simulation of the interacting  $\{J(r)\}$  loop segments, and their long-range interaction, would be of much interest, especially if the mean-loop diameter and loop self-energy at various scales are monitored.

Topological scaling ideas could be useful in other models, such as the anisotropic 3D  $XY$  model,<sup>13</sup> of interest in high- $T_c$  superconductors,<sup>14</sup> capacitive charging effects in the  $(2+1)D$  Josephson arrays and films,<sup>25</sup> hydrodynamic vortex loops in turbulence,<sup>11</sup> and dislocation loop pictures of melting.<sup>7(b)</sup> We hope to report on some of these applications elsewhere.

#### ACKNOWLEDGMENTS

It is a pleasure to thank the CSIR and UGC for partial support, and to acknowledge and thank Alex Chorin for providing material prior to publication, and Gary Williams for useful correspondence.

<sup>1</sup>V. Berezinskii, Zh. Eksp. Teor. Fiz. **61**, 1144 (1971) [Sov. Phys. JETP **34**, 610 (1971)].

<sup>2</sup>J. M. Kosterlitz and D. J. Thouless, J. Phys. C **6**, 1181 (1973).

<sup>3</sup>V. Ambegaokar, B. Halperin, D. Nelson, and E. Siggia, Phys. Rev. Lett. **40**, 783 (1978); V. Ambegaokar and S. Teitel, Phys. Rev. B **19**, 1667 (1979).

<sup>4</sup>B. Halperin and D. Nelson, J. Low Temp. Phys. **36**, 599 (1979).

<sup>5</sup>For reviews, see, e.g., (a) C. J. Lobb, Physica B + C **126B**, 319 (1984); (b) S. R. Shenoy (unpublished).

<sup>6</sup>D. Nelson, in *Phase Transition and Critical Phenomena*, edited by C. Domb and J. Lebowitz (Academic, New York, 1983), Vol. 7.

<sup>7</sup>(a) L. Onsager, Nuovo Cimento Suppl. **6**, 279 (1949); R. P. Feynman, in *Progress in Low Temperature Physics*, edited by C. Gorter (North-Holland, Amsterdam, 1955), Vol. 1; (b) W. Shockley, in *L'Etat Solid*, Proceedings of the Neuvième Conseil de Physique, Institute International de Physique Solvay (R. Stoops, Bruxelles, 1952).

<sup>8</sup>(a) G. A. Williams, Phys. Rev. Lett. **59**, 1926 (1987); **61**, 1142(E) (1988); (b) Physica B **165&166**, 769 (1990); (c) in *Excitations in 2D and 3D Quantum Fluids*, edited by A. G. F. Wyatt and H. J. Lauter (Plenum, New York, 1991); (d) J. Low Temp. Phys. **89**, 91 (1992).

<sup>9</sup>(a) S. R. Shenoy, Phys. Rev. B **40**, 5056 (1989); (b) **42**, 8595

- (1990).
- <sup>10</sup>(a) J. M. Kosterlitz, *J. Phys. C* **7**, 1046 (1974); (b) A. P. Young, *ibid.* **11**, L453 (1978).
- <sup>11</sup>A. J. Chorin and J. Akao, *Physica D* **52**, 403 (1991); A. J. Chorin, *J. Comp. Phys.* (to be published).
- <sup>12</sup>(a) C. Kawabata and K. Binder, *Annals Israel Phys. Soc.* **2**, 988 (1978); (b) W. Janke, Ph.D. thesis, Freie Universität, Berlin, 1985; (c) H. Kleinert, *Gauge Fields in Condensed Matter Physics*, Vol. I (World Scientific, Singapore, 1989).
- <sup>13</sup>(a) J. Epiney (unpublished); (b) W. Janke and T. Matsui, *Phys. Rev. B* **42**, 10 673 (1990); (c) A. Schmidt and T. Schneider, *Z. Phys. B* **87**, 265 (1992).
- <sup>14</sup>J. Friedel, *J. Phys. (Paris)* **49**, 1561 (1988); **49**, 1769 (1988); S. E. Korshunov, *Europhys. Lett.* **11**, 757 (1990); H. J. Jansen and P. Minnhagen, *Phys. Rev. Lett.* **66**, 1630 (1991); P. Minnhagen, *Helv. Phys. Acta* **65**, 205 (1992).
- <sup>15</sup>G. Kohring, R. Shrock, and P. Wills, *Phys. Rev. Lett.* **57**, 1358 (1986); G. Kohring and R. Shrock, *Nucl. Phys. B* **288**, 397 (1987).
- <sup>16</sup>(a) P. J. Flory, *Principles of Polymer Chemistry*, 6th ed. (Cornell University Press, Ithaca, NY, 1967), Chap. 14; (b) S. F. Edwards and P. Singh, Part I and S. F. Edwards and E. F. Jeffers, Part II, *J. Chem. Soc. Faraday Trans.* **2**, 1001 (1979); (c) M. Muthukumar and S. F. Edwards, in *Comprehensive Polymer Science*, edited by C. Booth and C. Price (Pergamon, New York, 1984), Vol. 2.
- <sup>17</sup>J. Gilliou and J. Zinn-Justin, *Phys. Rev. B* **21**, 3976 (1989).
- <sup>18</sup>R. Savit, *Phys. Rev. B* **17**, 1340 (1987).
- <sup>19</sup>In the context of the lattice superconductor, analogous to the 3D XY model, Y. H. Li and S. Teitel [*Phys. Rev. Lett.* **66**, 3301 (1991)] have shown that crossing can occur, with mutually perpendicular segments.
- <sup>20</sup>The ansatz is valid for the critical region  $l \leq l_-$  and  $l_- \gg 1$  only, "inside the fluctuations" and for the cores of the dominant loops. For the opposite hydrodynamic region, i.e., scales large compared to fluctuations, the core model is expected to break down. One finds  $\rho_l$  has further drops (magnified by  $e^l$  factors in the  $K_l$  and  $y_l$  plots) beyond the  $l$  region shown. However, these invalid regions are swept out to infinity as  $\epsilon \rightarrow 0$ , when the behavior shown remains the asymptotic behavior.
- <sup>21</sup>The critical coupling  $K_{0c}$  is actually that for 3D vortices in (2.2), rather than cosines of angles in (2.1). In 2D, the transition temperature  $T_{KT}$  is low, the spin wave (sw) low-temperature excitations are still well-defined, and their stiffness is nonzero, right up to  $T_{KT}$ . The minimum scale 2D vortex coupling, which determines  $T_{KT}$ , thus contains sw corrections. In 3D, however,  $T_c$  is much higher, the sw stiffness vanishes as  $\sim |T_c - T|^\nu$ , and such corrections may be small close to  $T_c$ .
- <sup>22</sup>N. Madras and A. Sokal, *J. Stat. Phys.* **50**, 109 (1988).
- <sup>23</sup>(a) J. Tobochnik and G. V. Chester, *Phys. Rev. B* **20**, 3761 (1979); (b) S. Miyashita, H. Nishimori, A. Kuroda, and M. Suzuki, *Prog. Theor. Phys.* **60**, 1669 (1978).
- <sup>24</sup>Y. Saito and H. Müller-Krumbhaar, *Phys. Rev. B* **23**, 308 (1981).
- <sup>25</sup>(a) L. Jacobs, J. V. José, M. A. Novotny, and A. M. Goldman, *Phys. Rev. B* **38**, 4562 (1988); (b) M. C. Cha, M. P. A. Fisher, S. M. Girvin, M. Wallin, and A. P. Young, *ibid.* **44**, 6883 (1991).